AIAA 94-0202
Ascent Flight Aerodynamic Characteristics of the National Launch System 1 1/2-Stage Launch Vehicle: NLS-2

A. Springer and D. Pokora
NASA Marshall Space Flight Center, Alabama

32nd Aerospace Sciences Meeting & Exhibit
January 10-13, 1994 / Reno, NV

ASCENT FLIGHT AERODYNAMIC CHARACTERISTICS OF THE NATIONAL LAUNCH SYSTEM 1 1/2-STAGE LAUNCH VEHICLE: NLS-2

A. Springer* and D. Pokora†
NASA Marshall Space Flight Center, Alabama

Abstract

The ascent flight aerodynamic characteristics of the National Launch System (NLS) 1 1/2-stage launch vehicle were determined. NASA is studying ways of assuring unmanned launch capabilities which are man rated to and from space by means other than the space shuttle. One launch system studied was the NLS. Two of the NLS vehicles proposed were the 1 1/2-stage vehicle and the Heavy Lift Launch Vehicle (HLLV). This paper discusses the 1 1/2-stage vehicle. To support the detailed configuration definition, two wind tunnel tests were conducted in the NASA Marshall Space Flight Center's 14×14-Inch Trisonic Wind Tunnel (TWT) during 1992. The tests were a static stability and a pressure test, each utilizing 0.004 scale models. The static stability test resulted in the forces and moments acting on the vehicle. The aerodynamics for the reference configuration with and without feedlines and an evaluation of three proposed engine shroud configurations were also determined. The pressure test resulted in pressure distributions over the reference vehicle with and without feedlines including the reference engine shrouds. These pressure distributions were integrated and balanced to the static stability coefficients resulting in distributed aerodynamic loads on the vehicle. The wind tunnel tests covered a Mach range of 0.60 to 4.96. These ascent flight aerodynamic characteristics provide the basis for trajectory and performance analysis, loads determination, and guidance and control evaluation.

Nomenclature

Symbol	Definition
$A_{b\,CS}$	Core projected base area, 646.2 ft^2 (z-y plane)
$A_{b\,ASRB}$	ASRB base area, 236.11 ft^2
Alpha	angle-of-attack, degrees
A_{ref}	reference area, 593.96 ft^2
ASRB	Advanced Solid Rocket Booster
Beta	angle-of-sideslip, degrees
C_A	axial force coefficient
C_l	rolling moment coefficient
C_M	pitching moment coefficient
C_N	normal force coefficient
C_n	yawing moment coefficients
C_P	pressure coefficient for tap P(n)
C_{P_b}	base pressure coefficient
C_Y	side force coefficient
D_{ref}	reference diameter, 27.5 ft
F_{A_T}	total axial force
$F_{AB_{ref}}$	base force, aerodynamic reference trajectory
L_{REF}	reference length, 27.5 ft
MACH	Mach number
MRP (X_T, Y_T, Z_T)	moment reference point, (4,385.5, 0, 0)
P	measured local pressure, psia
Pb	element base pressure, psia
Q	dynamic pressure, in lb/ft^2
S_{REF}	reference area, 593.96 ft^2
X_{CP}	model center of pressure, inches
$X_{1.5\text{ or HLLV}}$	vehicle axial location (full scale)
$X/L_{1.5\text{ or HLLV}}$	dimensionless distance from vehicle nose
$X_{M.S.}$	distance from vehicle nose in model scale

*Test Engineer, Member AIAA.
†Test Engineer

Introduction

The NLS is a joint NASA/Department of Defense (NASA/DOD) program to develop a family of launch vehicles that have common elements. Initially, this family consisted of an HLLV configuration designed to launch 100 to 150 klb payloads and a 1 1/2-stage vehicle to launch 50-klb payloads. This paper is limited to discussion of the 1 1/2-stage configuration.

To support the detailed configuration definition, two wind tunnel tests, TWT 733 and TWT 734, were run in MSFC's 14-Inch Trisonic Wind Tunnel facility to determine the effect of the different configurations on vehicle aerodynamics. TWT 733 was a static stability test that resulted in forces and moments for the 1 1/2-stage configuration. Variations in engine shroud design and the option of feedlines were studied. The second wind tunnel test, TWT 734, was a pressure test, which resulted in the pressure distributions for various conditions over the vehicle with and without feedlines. These data are to be utilized consistently with the force and moment results from TWT 733, thus insuring consistent data bases for trajectory, control, and loads systems studies. All test models are 0.004-scale.

The 1 1/2-stage vehicle consists of a cylindrical cargo element (the current Titan IV shroud) with a biconic nose cone and a 17°12' interstage mounted on

top of a modified Space Transportation System (STS) external tank (ET). Modifications to the ET consist of stretching the hydrogen tank and lox tank to accommodate the liquid propulsion system added to its base. This propulsion system consists of six space transportation main engines (STME's) with four engine shrouds. Figure 1 shows the 1 1/2-stage launch vehicle configuration static stability model in the MSFC 14×14-Inch Trisonic Wind Tunnel. Figure 2 depicts the NLS 1 1/2-stage vehicle geometry.

Test

Facility Description

The MSFC 14×14-Inch Trisonic Wind Tunnel is an intermittent blowdown tunnel which operates by high pressure air flowing from storage to either vacuum or atmosphere conditions. The transonic test section provides a Mach number range from 0.2 to 2.0. Mach numbers between 0.2 and 0.9 are obtained by using a controllable diffuser. The Mach range from 0.95 and 1.3 is achieved through the use of plenum suction and perforated walls. Each Mach number above 1.30 requires a specific set of two-dimensional contoured nozzle blocks. A solid-wall supersonic test section provides the entire range from 2.74 to 5.0 with one set of automatically actuated contour blocks. Air is supplied to a 6,000 ft^3 storage tank at approximately –40 °F dew point and 425 psig. The compressor is a three-stage reciprocating unit driven by a 1,500-hp motor. The tunnel flow is established and controlled with a servo-actuated gate valve. The controlled air flows through the valve diffuser into the stilling chamber and heat exchanger where the air temperature can be controlled from ambient to approximately 180 °F. The air then passes through the test section, which contains the nozzle blocks and test region.

Downstream of the test section is a hydraulically controlled pitch sector that provides the capability of testing up to 20 angles-of-attack from –10° to +10° during each run. Sting offsets are available from obtaining various maximum angles-of-attack up to 90°. The diffuser section has movable floor and ceiling panels which are the primary means of controlling the subsonic Mach numbers and permit more efficient running supersonically. Tunnel flow is exhausted through an acoustically damped tower to atmosphere or into the vacuum field of 42,000 ft^3. The vacuum tanks are evacuated by vacuum pumps driven by a total of 500 hp.

The data acquisition system is a Hewlett-Packard (HP) 349A controller with an HP 3456A digitizer. The unit is equipped with various control modules for facility system control, angle-of-attack readout, Scanivalve control, etc. Currently, the system is configured to 40 low-level strain gauge, thermocouple, or pressure channels per second, with a 2- or 3-s recycle time to change angle-of-attack and allow for settling. Low pass filters are available for all channels and are routinely used on strain gauge balance channels. System control and data reduction are by an HP 200-series computer with a 1-Mbyte memory. Data are reduced after each run, and tabulated data are available in about 20 s using an HP laser jet printer. All data are stored on disk for subsequent transfer to another computer for further analysis or data base construction.

On-line data are reduced to coefficient form by a solid-state data acquisition and computing system. Hard copies of tabulated data and preliminary plots are provided a few minutes after each run. More detailed information on the 14-Inch TWT is contained in reference 1.

Model Descriptions

The 1 1/2-stage vehicle models consist of a cylindrical payload section 2.88 inches in length, 0.800 inch in diameter with a biconic nose cone (15°/25°). The interstage section (0.838 inch in length) connects the payload section to an ET section which has been modified to include an additional 5 ft in length (the ET section including the propulsion module is 7.647 inches in length and 1.324 inches in diameter). The reference configuration engine shrouds are made to be removable and are 0.692 inch in length and have a 0.252-inch radius. A 1 1/2-stage optimum shroud design, 0.882 inch in length and 0.662 inch in radius, was also tested. The HLLV optimum shroud design, 0.682 inch in length and 0.662 inch in radius, was also tested on the 1 1/2-stage configuration. The model utilizes removable feedlines which are 5.28 inches in length with side extensions 110° from the centerline blending into the engine shrouds. Figure 3 depicts the three engine shroud configurations tested for the 1 1/2-stage configuration. Due to the complexity of fabrication/assembly/cost, existing stock materials were utilized for the lox feedlines. Therefore, the dimensions for the feedlines do not correspond exactly to the reference configuration feedline dimensions. The effects are considered to be small on the total vehicle aerodynamics. For plume simulation, a solid plume and a flat plate were utilized to match analytically determined values. Model dimensions are identical for the static stability and pressure models. The solid plume simulator can be seen in Fig. 1, the frustum mounted to the sting aft of the base of the vehicle.

The 1 1/2-stage configuration pressure model was instrumented with 233 pressure taps located at various stations shown in Fig. 4. Ports were nominally placed at 22.5° increments in quadrants I and III. This setup allowed for a full set of pressure data to be obtained with the fewest taps. The locations of ports at an example station is shown in Fig. 5. A closeup of the nose region of the pressure model is shown in Fig. 6. Two taps were found to be bad and were deleted from the data. These taps were not seen to be detrimental to the test, so the test proceeded without them.

Test Procedure

For both tests, testing was done over a Mach range of 0.6 to 4.96. The angle-of-attack and angle-of-sideslip ranges for each run were –8° to +8° for the static stability test and –4° to +8° for the pressure test, both in 2° increments.

The test schedule involved testing each configuration for a predetermined, standard set of 13 Mach numbers.

The pressure test required two sets of pressure tap data to obtain a full set of vehicle pressure coefficients. This is due to the limited number of pressure transducers in the data acquisition system. The tap hookups are defined as hookup/tapset A and hookup/tapset B. Setup A is the forward part of the vehicle past the frustum, ring 1 to 18, including all the taps at phi angles of 0°, 90°, 180°, and 270° along the whole vehicle. Setup B is the aft part of the vehicle ring 14 to 28 including all the taps at phi angles of 0°, 90°, 180°, and 270° along the whole vehicle.

Solid Plume Simulation

Plume studies were done for the $1^1/_2$-stage reference configuration for the static stability and pressure tests over the entire Mach range. The plume locations for each test were measured from the base of the vehicle. A study was also done, during the pressure test, to determine the base pressures for which plume induced flow separation occurred on the vehicle and how far forward the separation occurred. The results from this study are presented in reference 2. The simulated plume for the $1^1/_2$-stage vehicle is shown in Fig. 1. The general study used the solid plume alone up to Mach 1.96 and added the flat plate at the higher Mach numbers. The separation study used the plume with the flat plate reversed, so the flat plate was toward the vehicle, allowing the highest pressure to be obtained.

Instrumentation and Data Reduction

Static Stability Measurements

The six-component balance on which the model was mounted measured total mated vehicle forces and moments. Six-component force and moment coefficients were computed from the main balance about the axis system and then transferred to the moment reference point shown in Fig. 7. Forebody coefficients were calculated using the element base pressure results. Angles-of-attack and angles-of-sideslip were calculated from the sector reading, taking into account the sting and balance deflections determined using pretest calibrations.

Pressure Measurements

Model base pressures were measured using external tubes placed next to the base of each element, and are sampled by transducers mounted outside the test section as are all other measurements. The same position/proximity for both tests were used.

The pressure model used 0.032-inch tubing for the pressure taps converted to 0.064 for the data acquisition system.

All pressure data were reduced to coefficient form as follows:

$$CP(n) = (P(n)-Pinf)/Qinf\,; \quad n = 1 \text{ -> } 233$$

Results

Static Stability Test

The $1^1/_2$-stage aerodynamic data base consists of vehicle data including plume effects. These data were determined as a result of the test performed in the MSFC 14-Inch Trisonic Wind Tunnel.[3] The data (forces and moments) are to be applied at the moment reference point (MRP). Figure 7 shows the aerodynamic axis system for the data base. The MRP for which the data base originates is shown to be located at the base of the vehicle (Fig. 7).

The data base contains the force and moment coefficients linearized as slopes/intercepts of the longitudinal data with respect to alpha and of the lateral data with respect to beta. The coefficients of the longitudinal data are normal force, C_N, pitching moment, C_M, and axial force, C_A. The coefficients of the lateral data are side force, C_Y, yawing moment, C_n, and rolling moment, C_l. C_l for this configuration is essentially zero due the symmetry of the vehicle. Figures 8 through 12 show the aerodynamic coefficients versus Mach for the $1^1/_2$-stage configuration.

If a force/moment is desired, the aerodynamic coefficients can be converted using the following equations:

$$\text{Force} = \text{Coeff.}\ (C_N, C_A, C_Y) * Q * A_{\text{ref}}$$

$$\text{Moment} = \text{Coeff.}\ (C_M, C_n, C_l) * Q * A_{\text{ref}} * D_{\text{ref}}\ .$$

Base axial force data, FAB (klb) as a function of altitude (kft), dynamic pressure, Q, thrust (lb), and Mach was determined. The base force is based on the $1^1/_2$-stage reference ascent flight trajectory. Base axial force, FAB versus altitude is shown in Fig. 13. Figure 14 shows reference dynamic pressure versus altitude. The total axial force is determined by the sum of the base axial force and the forebody axial force as shown in the following.

$$F_{A_T} = C_{A_o} * Q * A_{ref} + F_{AB_{ref}}$$

Pressure Test

The pressure test resulted in 231 individual pressure coefficients over the body of the vehicle for the range of Mach numbers and angles-of-attack tested. Extraneous points were removed from the data. The resulting data sets were interpreted to even angle-of-attack. These data were then mirrored to cover the surface of the vehicle. At points where data were lacking, due to the number of taps or a bad data point, the surrounding data were used to spline the missing data into the data set.

Distributed Loads

Normal force coefficient slope with respect to angle-of-attack, $\frac{dC_N}{d(X/D)}$, pitching moment coefficient slope with respect to angle-of-attack, $\frac{dC_M}{d(X/D)}$, and axial force coefficient, $\frac{dC_A}{d(X/D)}$ distributions have been generated for the $1^1/_2$-stage vehicle configuration of the NLS. Distributed loads were determined over the transonic Mach range.

A normal force coefficient slope distribution and pitching moment coefficient slope distribution were created using pressure data from reference 4 integrated and matched to data from reference 3. This ensures consistency between the aerodynamic data used for performance, trajectory, control, and loads studies. The running load distributions were balanced to the data in reference 3 to nominally within 10 percent (5-percent normal force and 10-percent pitching moment). No criteria have yet been established requiring a closer balance between forces/moment data and load distributions. The balancing and integration of the data were done using the following Macintosh programs: MCP™, pressure data integration and initial distributed loads; Kaleidagraph™, integration of distributed loads; Excel™, data analysis; and DeltaGraph Professional™, plotting of data. Figure 7 shows the aerodynamic axis system for the $1^1/_2$-stage vehicle and defines the reference dimensions utilized in the data base.

The axial force coefficient distribution also was created using the preceding methods. The axial force coefficient running load distributions were balanced to the data in reference 3 to within 5.0 percent.

The preceding data sets can be used to determine the local normal force distribution, local pitching moment distribution, local axial force distribution, and component loading on the vehicle. The force is determined by:

$$\text{Local Normal Force} = C_{NA} * Q * S_{REF} * \text{Alpha} \ ,$$

$$\text{Local Axial Force} = C_A * Q * S_{REF} * \text{Alpha} \ ,$$

where C_{NA} is the normal force coefficient slope, C_A is the axial force coefficient, Q is the dynamic pressure, S_{REF} is the reference area, and alpha is the angle-of-attack. The loading on a component of the vehicle (e.g., interstage) is determined by integration of the distribution over the component.

$$\frac{dC_N}{d(X/D)} = \frac{dC_{Na}}{d(X/D)} * a \ ,$$

and

$$C_N = \int_{X_{Start}}^{X_{End}} \frac{dC_N}{d(X/D)} \, d\frac{X}{D} \ ,$$

$$\text{Component Normal Force} = C_N * Q * S_{Ref} \ .$$

These distributed loads do not include the engine shroud loads. The engine shroud contributions are represented by incremental point loads placed at station 4360 or at an X/D of 9.254 (Fig. 15). The base of the vehicle is station 4385.5.

The total normal force is determined using the above formula and integrating over the whole vehicle, not just a single component and then adding in the engine shroud increments.

$$C_A = \int_{X_{Start}}^{X_{End}} \frac{dC_A}{d(X/D)} \, d\frac{X}{D} \ .$$

The data can be converted to a new dimension format other than *X/D* by multiplying by the required ratio. To convert to *X/L*, multiply the *X/D* location by *D/L* (reference diameter divided by reference length). To convert to station location, multiply the *X/D* location by *D*, reference diameter, resulting in length from the nose. It should be noted that integration using the *X/D* location is required to obtain the correct total normal force coefficient or axial force coefficient. This is a result of the data being $dCNa/d(X/D)$ and $dCA/d(X/D)$. Changing dimension formats will result in incorrect integration when using the *CNA* and *CA* values, and new coefficients must be determined to match the new dimensions.

Normal force coefficient slope distribution data, pitching moment coefficient slope distribution data, and axial force coefficient distribution data for the $1^1/_2$ stage configuration are given in graphical form for the transonic Mach range. Distributed loads for Mach number of 0.6, 0.8, 0.9, 0.95, 1.05, 1.1, 1.25 and 1.46 were determined. This Mach range encompasses the typical maximum dynamic pressure ascent loading conditions. References 3 and 4 also contain data for Mach numbers of 1.96, 2.74, and 3.48. During the NLS program, there was no requirement for distributions at these Mach numbers.

Figures 16 through 18 present the normal force coefficient slope distribution data, Figs. 19 through 21 present the pitching moment coefficient slope distribution data, and Figs. 22 through 24 present the axial force coefficient distribution data graphically. The distributions are plotted against vehicle station number divided by the reference diameter of the vehicle (X/D). These graphic representations were done using a spline function connecting the data points, which resulted in some undesirable trends between data points. These trends are obvious and should be disregarded. The actual integration and balancing analysis were done using a linear interpolation between the data points.

The shroud increments given at the bottom of the distribution tables were determined from reference 3 and are added to the distribution totals to obtain the total coefficient loads for the vehicle including shrouds. The shroud increments are for four shrouds. These increments are applied at station 4360 or at an X/D of 9.254 (Fig. 15).

The data bases resulting from the wind tunnel tests performed at MSFC's 14-Inch Trisonic Wind Tunnel provide the basis for detailed vehicle analysis.

Conclusions

These two wind tunnel tests, in support of the detailed configuration definition, were conducted in the NASA MSFC's 14×14-Inch Trisonic Wind Tunnel during 1992. The static stability and a pressure test each utilized 0.004 scale models. The static stability test resulted in the forces and moments acting on the vehicle. The aerodynamics for the reference configuration with and without feedlines and an evaluation of three proposed engine shroud configurations were also determined. The pressure test resulted in pressure distributions over the reference vehicle with and without feedlines including the reference engine shrouds. These pressure distributions were integrated and balanced to the static stability coefficients resulting in distributed aerodynamic loads on the vehicle. The wind tunnel tests covered a Mach range of 0.60 to 4.96.

The location and geometry of the engine shrouds tested is shown in Fig. 25. A set of four shrouds at 45° spacing were mounted to the vehicle for each configuration. The effects of the three engine shrouds on the longitudinal aerodynamic characteristics of the $1^1/_2$-stage configuration are shown in Figs. 26 and 27. From these figures, it is seen that the larger the angle, the greater the increase in drag. A slight change in normal force is seen, but this results in no noticeable change in pitching moment due to the moment reference point being located at the base of the vehicle. A 15-percent decrease in total vehicle drag can be seen by using an optimum aerodynamic engine shroud design.

The effects of feedlines, reference engine shrouds, and their component increments of the aerodynamic characteristics are shown in Figs. 8 through 12 and 25 through 28. Feedlines have little effect on vehicle drag when compared to the effect of engine shrouds which is approximately 25 percent of the total vehicle drag. Feedlines, on the other hand, have a relatively large effect on the lateral characteristics of the vehicle. The effect of feedlines and shrouds on the center of pressure on the vehicle is shown in Fig. 28. The clean vehicle's center of pressure is moved aft with addition of feedlines and engine shrouds. Engine shrouds account for this movement aft. Feedlines reduce the aft movement of the center of pressure due to the engine shrouds. The center of pressure of the vehicle can be moved aft through the addition of feedlines and engine shrouds. The magnitude of this movement is affected by the application of these elements. Through sizing these elements and the possible addition of fins, the desired center of pressure can be obtained.

The NLS aerodynamic data was used by the Trajectory and Performance Group, the Loads Analysis Group, and the Guidance and Control Group at MSFC in the design study of the $1^1/_2$-stage vehicle. These data are applicable for use to other similar configurations that may be developed.

The data resultant from these tests verified earlier predicted theoretical and analytical models. The data obtained from these tests provide a generic matrix of data on a symmetric inline launch vehicle. The full data base also provides increments for engine shroud and feedline effects. These data, the data base, and incremental data, when combined with the distributed loads provide a firm basis for analytical programs or computational fluid dynamic bench mark studies over the full range of subsonic, transonic, and supersonic Mach numbers. Future tests and studies can benefit from the data generated from these tests.

Acknowledgments

The authors would like to thank the wind tunnel test team at Marshall Space Flight Center for their help in making these wind tunnel tests a success: Mr. H. Brewster, Mr. H. Gwin, Ms. S. Espey, Mr. A. Frost, Mr. C. Dill, Mr. J. Heaman, and Ms. M. Niedermeyer.

References

1. "National Launch System (NLS) Reference System Definition," EE81(026-91), May 28, 1991.

2. Springer, Anthony M.: "Experimental Investigation of Plume-Induced Flow Separation on the National Launch System (NLS) $1^1/_2$-Stage Launch Vehicle." AIAA 94-0030, January 1994.

3. Pokora, Darlene C.: "Posttest Report for the National Launch System (NLS) in the MSFC 14-Inch Trisonic Wind Tunnel." ED34-04-93, March 15, 1993.

4. Springer, Anthony M.: "Post-Test Report for TWT 734 The National Launch System (NLS) $1^1/_2$-Stage Pressure Test in the MSFC 14-Inch Trisonic Wind Tunnel." ED35-127-92, September 3, 1992.

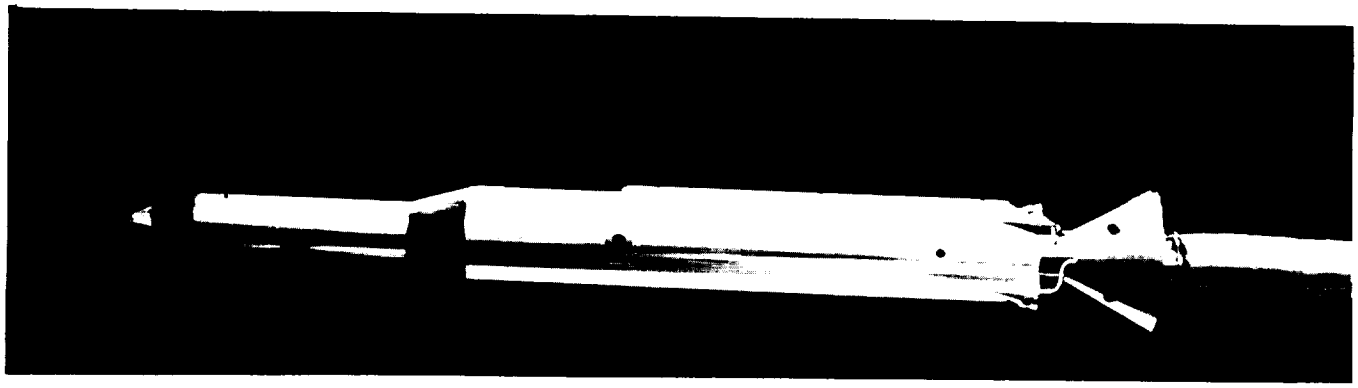

Fig. 1. NLS 1 1/2-Stage Vehicle Static Stability Model Mounted in the MSFC 14x14-Inch Trisonic Wind Tunnel.

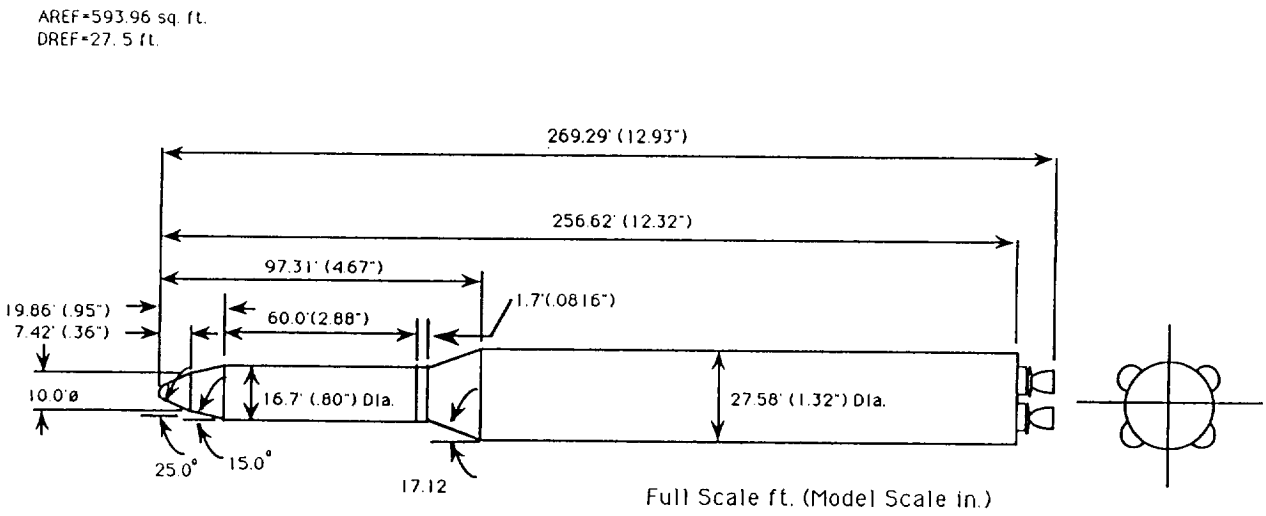

Fig. 2. NLS 1 1/2-Stage Vehicle Geometry.

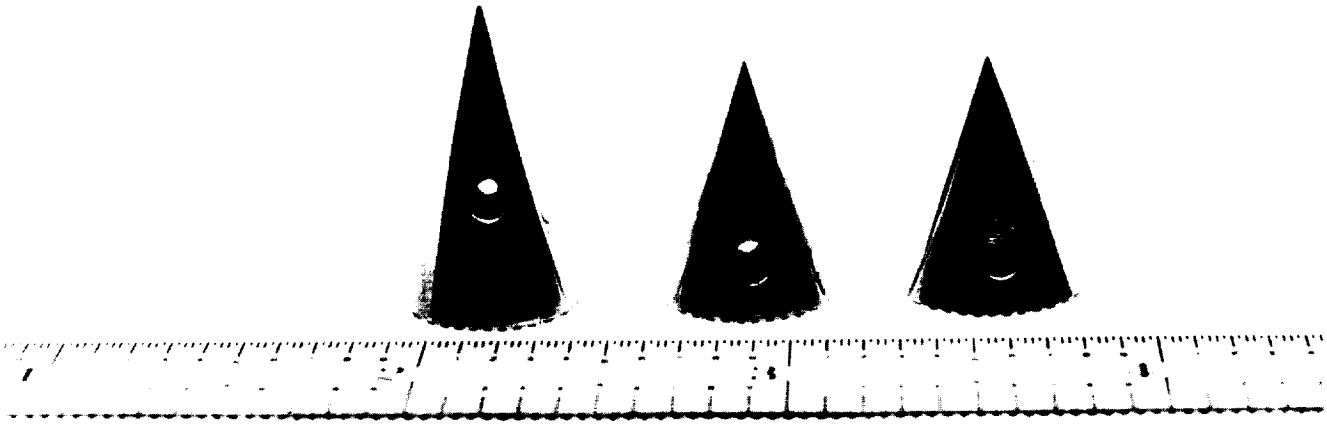

Fig. 3. Engine Shroud Configurations Tested.

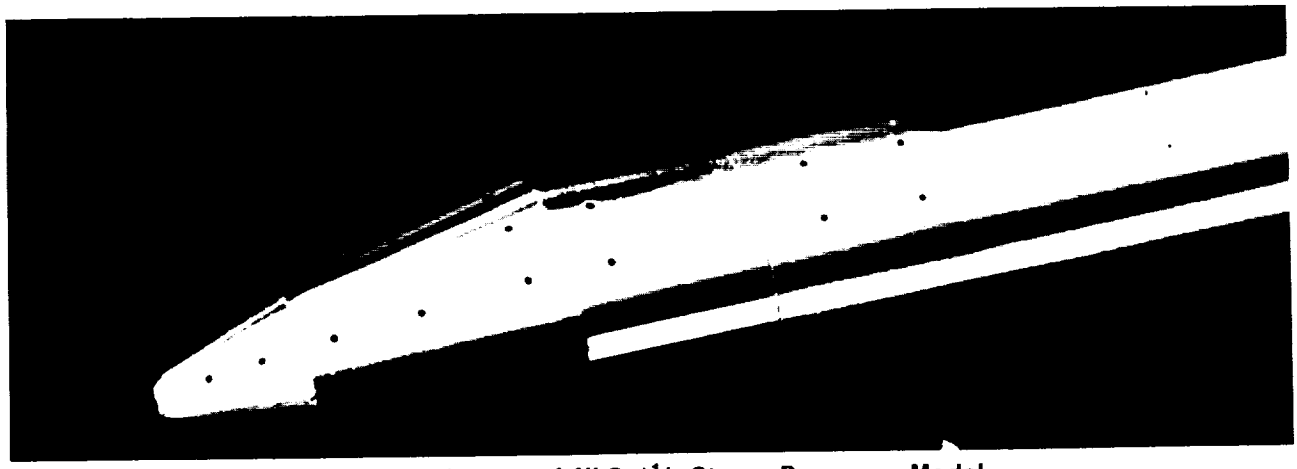

Fig. 4. Closeup of NLS 1 1/2-Stage Pressure Model.

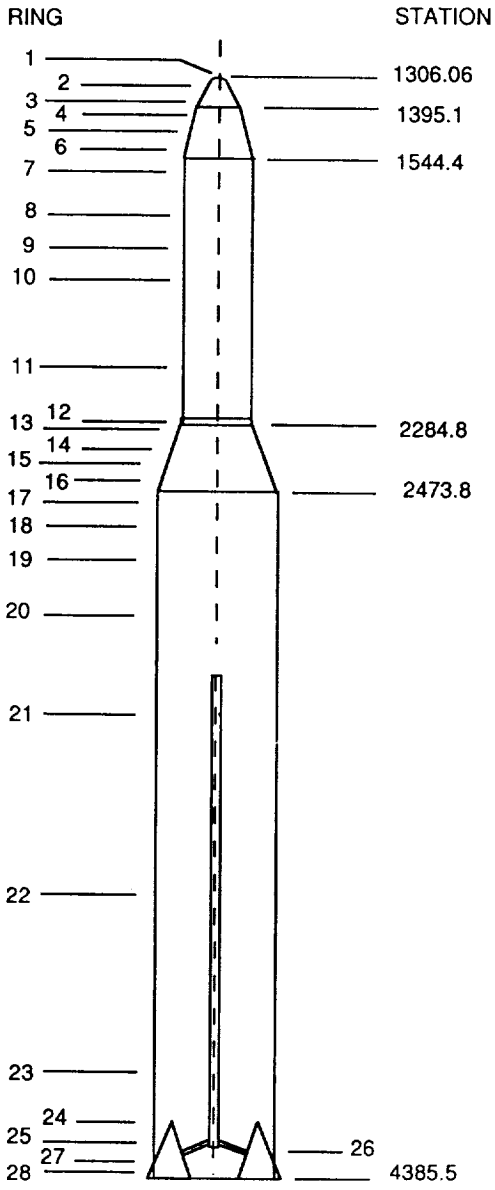

Fig. 5. Ring Locatin of Pressure Tap Stations.

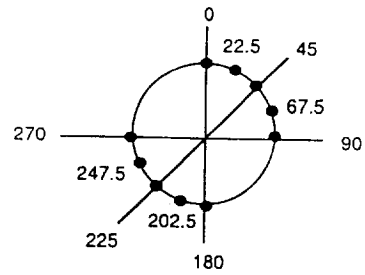

Fig. 6. Example Pressure Tap Phi Locations at a Given Station.

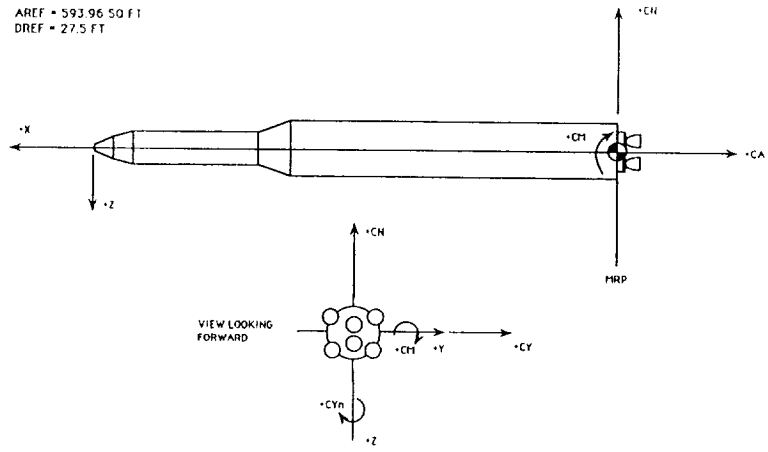

Fig. 7. Aerodynamic Axis System.

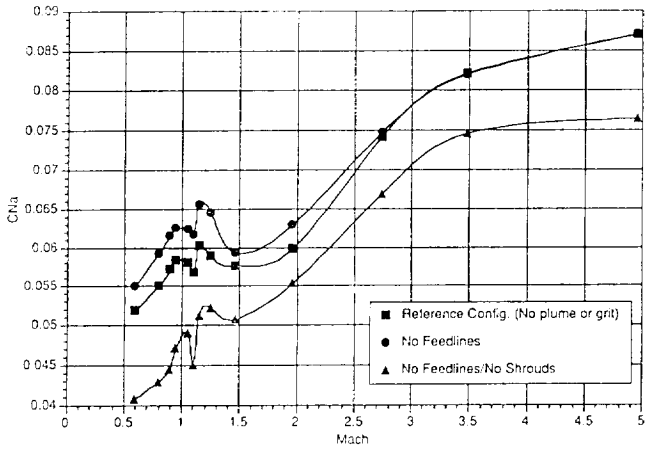

Fig. 8. CNa Versus Mach Number.

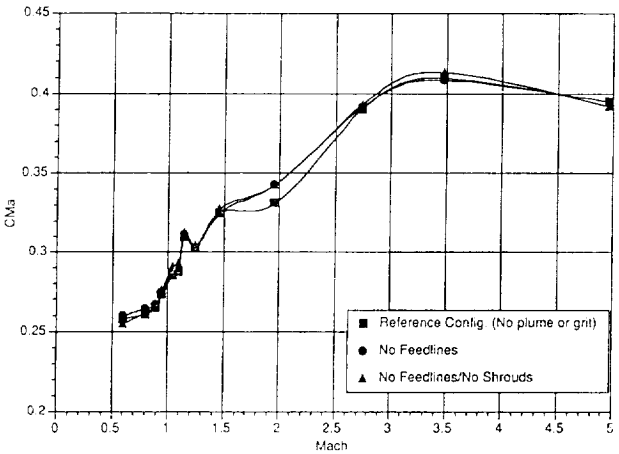

Fig. 9. CMa Versus Mach Number.

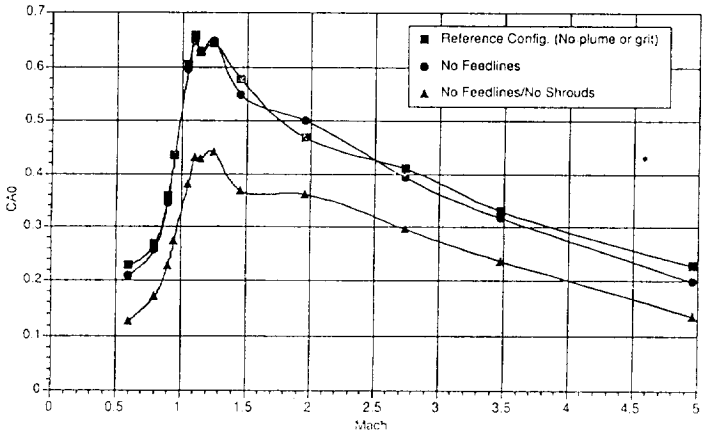

Fig. 10. CAO Versus Mach Number.

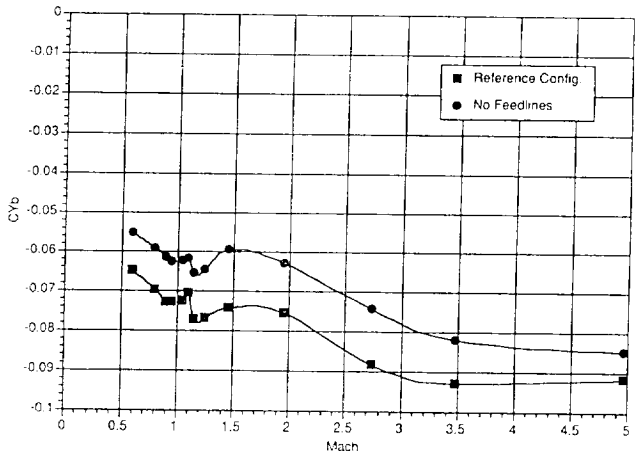

Fig. 11. CYb Versus Mach Number.

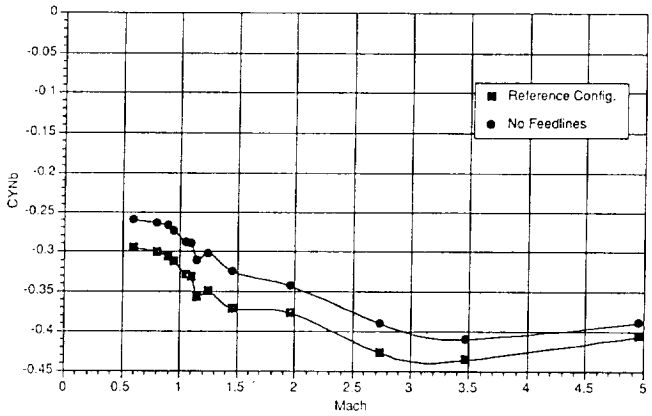

Fig. 12. CYNb Versus Mach Number.

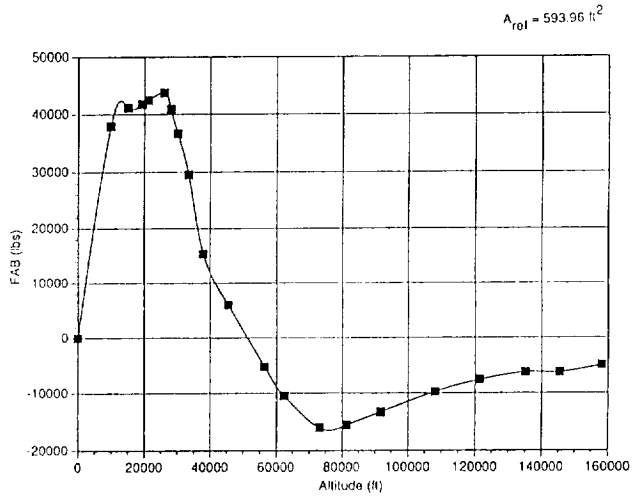

Fig. 13. Base Axial Force (FAB) Versus Altitude.

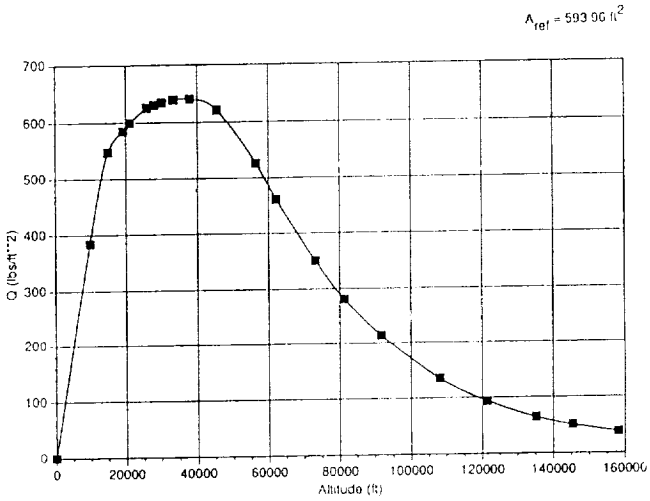

Fig. 14. Dynamic Pressure (Q) Versus Altitude.

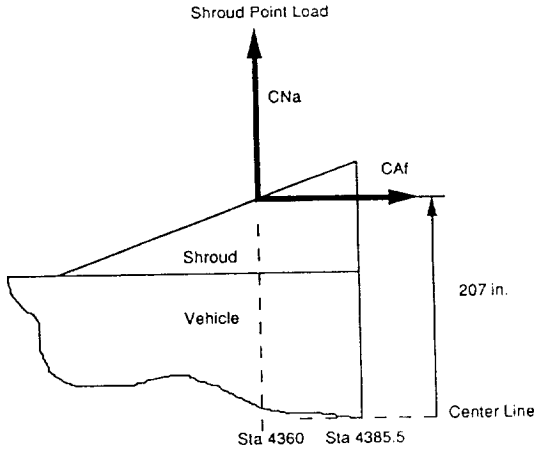

Fig. 15. Shroud Increment.

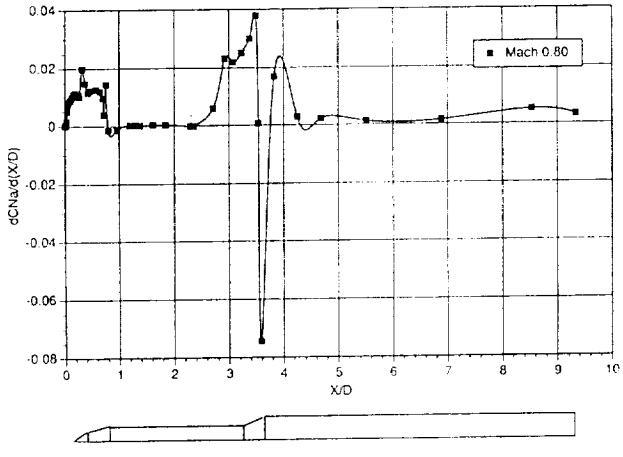

Fig. 16. NLS 1^1/$_2$-Stage, Mach 0.80, dCNa Versus X/D.

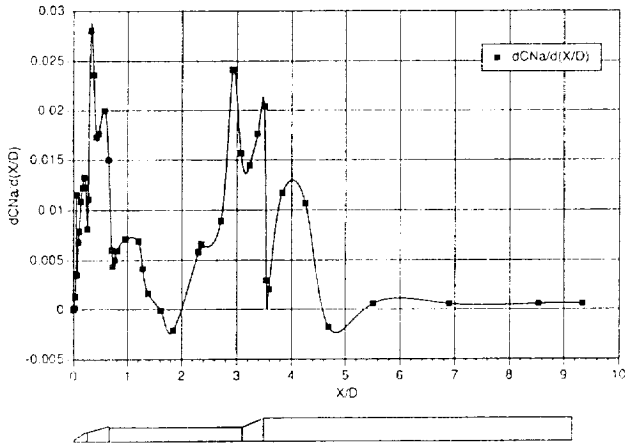

Fig. 17. NLS 1^1/$_2$-Stage, Mach 1.05, dCNa Versus X/D.

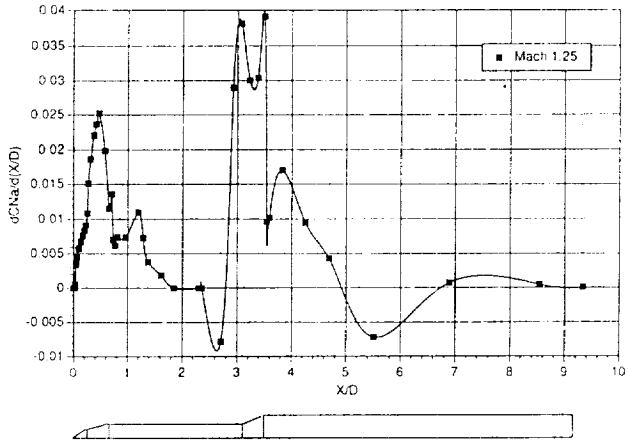

Fig. 18. NLS 1^1/$_2$-Stage, Mach 1.25, dCNa Versus X/D.

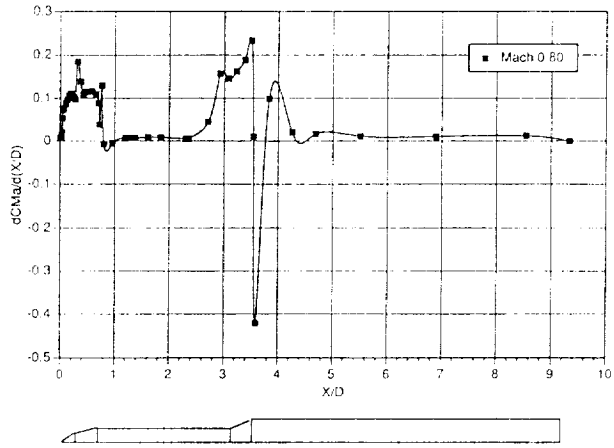

Fig. 19. NLS 1^1/$_2$-Stage, Mach 0.80, dCMa Versus X/D.

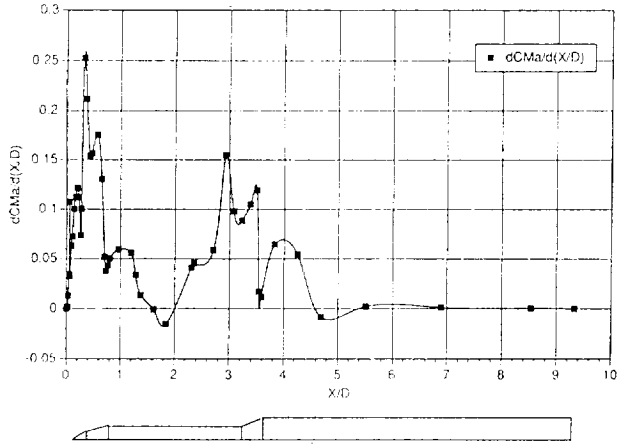

Fig. 20. NLS 1 1/2-Stage, Mach 1.05, dCMa Versus X/D.

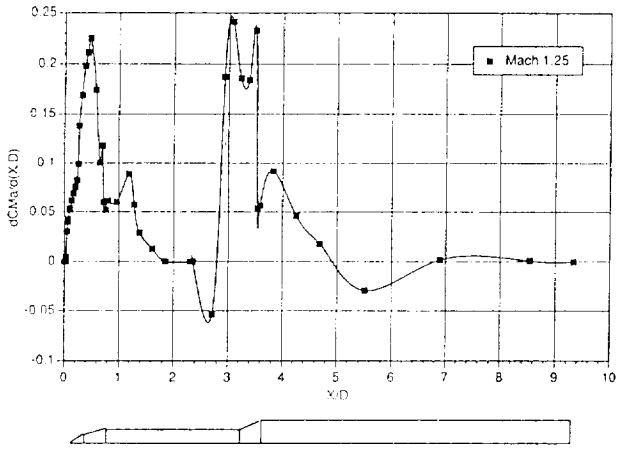

Fig. 21. NLS 1 1/2-Stage, Mach 1.25, dCMa Versus X/D.

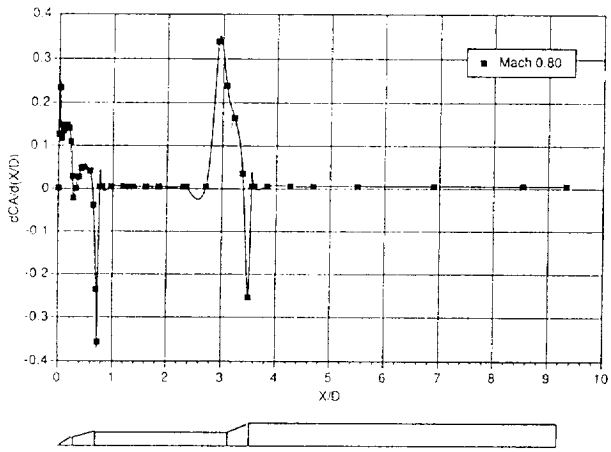

Fig. 22. NLS 1 1/2-Stage, Mach 0.80, dCA Versus X/D.

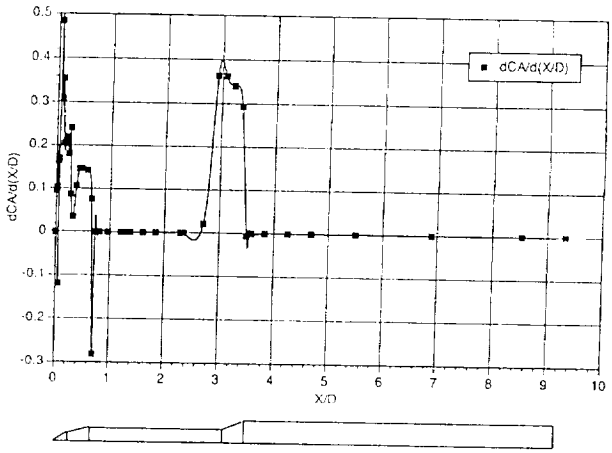

Fig. 23. NLS 1 1/2-Stage, Mach 1.05, dCA Versus X/D.

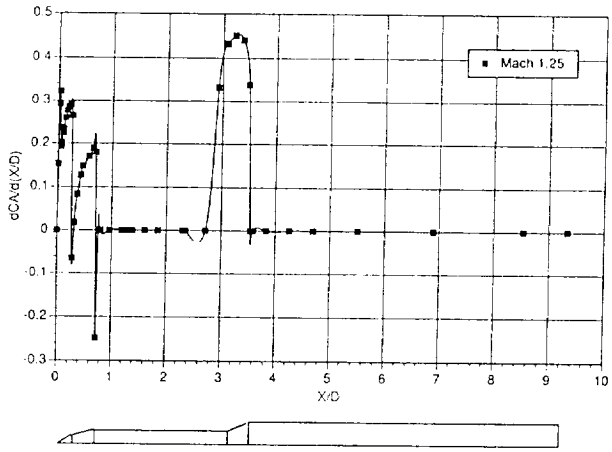

Fig. 24. NLS 1 1/2-Stage, Mach 1.25, dCA Versus X/D.

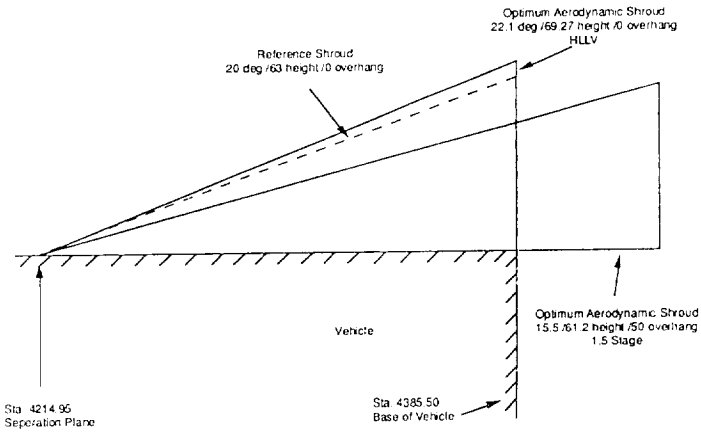

Fig. 25. NLS Shroud Layout.

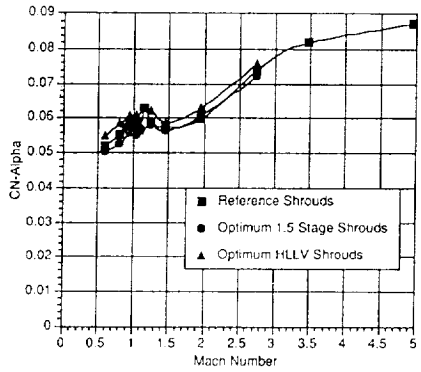

Fig. 26. NLS 1.5-Stage Configuration, CNA Versus Mach Number.

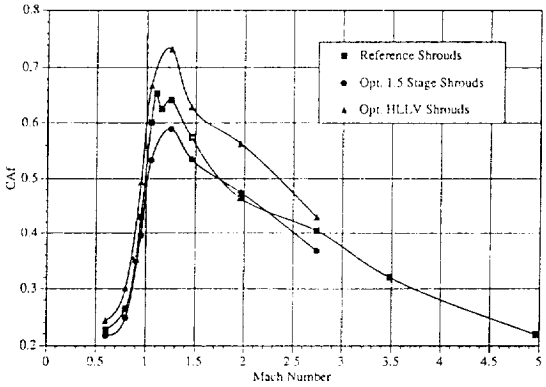

Fig. 27. 1.5-Stage Configuration, Forebody Axial Force Versus Mach Number.

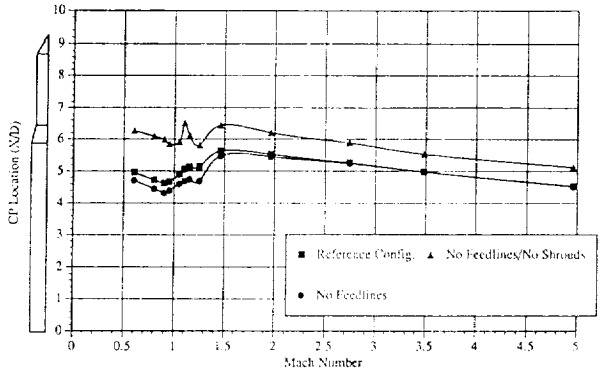

Fig. 28. CP Variation With Mach Number, 1.5-Stage Vehicle With Reference Shrouds.